Visible laser emission of solid state pumped LiLuF$_4$:Pr^{3+}

F. Cornacchia

NEST and Scuola Normale Superiore, Piazza dei Cavalieri 7, 56126 Pisa, Italy

francesco.cornacchia@df.unipi.it

A. Richter, E. Heumann, and G. Huber

Institute of Laser Physics, University of Hamburg, Luruper Chaussee 149, D-22761 Hamburg, Germany

andricht@physnet.uni-hamburg.de

D. Parisi, and M. Tonelli

NEST and Dipartimento di Fisica dell'Università di Pisa, Largo B. Pontecorvo 3, 56127 Pisa, Italy

http://www.df.unipi.it/ nmla

Abstract: In the present work we report on the growth, spectroscopy and laser results of LiLuF$_4$:Pr^{3+} 1.25% in the melt. Room temperature polarized absorption and emission spectra have been recorded and the decay time of the $^3P_0$ manifold has been measured. Finally efficient room temperature laser emission have been obtained at 522.8 nm, 607.25 nm, 640.17 nm and 721.5 nm under 480 nm pumping by means of an optically pumped semiconductor laser.

© 2007 Optical Society of America

References and links

1. S. Nicolas, E. Decroix, Y. Guyot, M.-F. Joubert, R. Yu. Abdulsabirov, S. L. Korapleva, A. K. Naumov, and V. V. Semashko, "4f^2 to 4f5d excited state absorption in Pr^{3+}-doped crystals," Opt. Mater. **16**, 233-242 (2001).
2. G. Özen, O. Forte, and B. Di Bartolo, "Downconversion and upconversion dynamics in Pr-doped Y$_3$Al$_5$O$_{12}$ crystals," J. Appl. Phys. **97**, 013510 (2005).
3. G. Özen, O. Forte, and B. Di Bartolo, "Upconversion dynamics in Pr-doped YAlO$_3$ and Y$_3$Al$_5$O$_{12}$ laser crystals," Opt. Mater. **27**, 1664-1671 (2005).
4. U. Hömmerich, E. Brown, P. Amedzake, S. B. Trivedi, and J. M. Zavada, "Mid-infrared (4.6 μm) emission properties of Pr^{3+} doped KPb$_2$Br$_5$," J. Appl. Phys. **100**, 113507 (2006).
5. N. V. Kuleshov, A. S. Shinkevich, V. G. Shcherbitsky, V.P. Mikhailov, T. Danger, T. Sandrock, and G. Huber, "Luminescence and time-resolved excited state absorption measurements in Pr^{3+}-doped La$_2$Be$_2$O$_5$ and KGd(WO$_4$)$_2$ crystals," Opt. Mater. **5**, 111-118 (1996).
6. N. V. Kuleshov, V. G. Shcherbitsky, A. A. Lagatsky, V. P. Mikhailov, B. I. Minkovb, T. Danger, T. Sandrock, and G. Huber, "Spectroscopy, excited-state absorption and stimulated emission in Pr^{3+}-doped Gd$_2$SiO$_5$ and Y$_2$SiO$_5$ crystals," J. Lumin. **71**, 27-35 (1997).
7. F. Xiong, X. Lin, Z. Luo, Q. Tan, E. Ma, and Y. Huang, "Spectroscopic properties of Pr^{3+} ions in biaxial LaB$_3$O$_6$ crystal," J. Appl. Phys. **99**, 064905 (2006).
8. X. Lu, Z. You, J. Li, Z. Zhu, G. Jia, B. Wu, and C. Tu, "Optic characteristics of Pr^{3+} doped NaY(MoO$_2$)$_2$ crystal," Appl. Phys. B **85**, 585-589 (2006).
9. T. Danger, A. Bleckmann, and G. Huber, " Stimulated emission and laser action of Pr^{3+}-doped YA1O$_3$," Appl. Phys. B **58**, 413-420 (1994).

10. L. Esterovitz, R. Allen, M. Kruer, F. Bartoli, L. S. Goldberg, H. P. Jenssen, A. Linz, and V. O. Nicolai, "Blue light emission by a Pr:LiYF$_4$ laser operated at room temperature," J. Appl. Phys. **48**, 650-652 (1977).
11. T. Sandrock, T. Danger, E. Heumann, G. Huber, and B. H. T. Chai, "Efficient Continuous Wave-Laser Emission of Pr^{3+}-Doped Fluorides at Room Temperature," Appl. Phys. B **58**, 149-151 (1994).
12. A. A. Kaminskii, A. I. Lyashenko, N. P. Isaev, V. N. Karlov, V. L. Pavlovich, S. N. Bagaev, A. V. Butashin, and L. E. Li, "Quasi-cw Pr^{3+}:LiYF$_4$ laser with λ=0.6395 μm and an average output power of 2.3 W," Quantum Electron. **28**, 187-188 (1998).
13. A. Richter, E. Heumann, E. Osiac, G. Huber, W. Seelert, and A. Diening, "Diode pumping of a continuous-wave Pr^{3+}-doped LiYF$_4$ laser," Opt. Lett. **29**, 2638-2670 (2004).
14. A. Richter, N. Pavel, E. Heumann, G. Huber, D. Parisi, A. Toncelli, M. Tonelli, A. Diening, and W. Seelert, "Continuous-wave ultraviolet generation at 320 nm by intracavity frequency doubling of red-emitting Praseodymium lasers," Opt. Express **14**, 3282-3287 (2006).
15. A. Yoshikawa, K. Kamada, M. Nikl, K. Aoki, H. Sato, J. Pejchal, and T. Fukuda, "Growth and luminescent properties of Pr:KY$_3$F$_{10}$ single crystal," J. Cryst. Growth **285**, 445-449 (2005).

1. Introduction

In the recent years a lot of interest has grown for the development of all-solid state laser sources emitting in the visible region of the electromagnetic spectrum. The perspective for such devices are linked to the development of a new generation of colour displays, new data storage techniques, holographic techniques, calibration stars for astrophysical experiments, and also in biomedical applications tasks.

For that purpose, one of the most promising candidates between rare earth ions is Pr^{3+}. The electronic configuration of Pr is [Xe](closed shell)+4f^2, and the energy level scheme is reported in Fig. 1 for the LiLuF$_4$ crystalline host [1]. Looking to Fig. 1 it is clear that a large number of potential laser transitions are available practically throughout the whole visible range up to the infrared. In the same Figure, we show in blue the pump wavelength, and in green, orange, red, and dark-red the different laser transitions that will be analysed in the next sections. Pr^{3+}-doped materials are also attractive as up-conversion, potential tunable UV, and vacuum
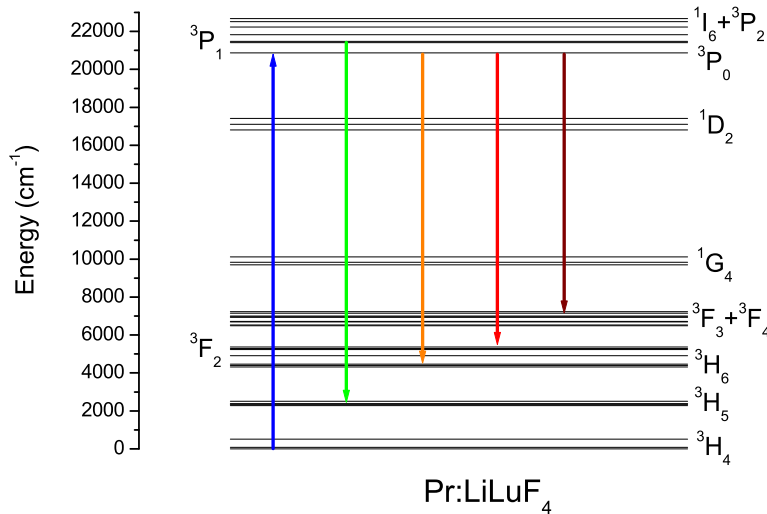

Fig. 1. Energy level scheme of Pr:LLF. In blue the pumping laser at 479.5 nm, and in other colors the laser transitions under analysis. Energy level position after Ref. [1].

ultraviolet VUV solid state laser media [1, 2, 3] as well as mid-infrared applications in low phonon materials [4].

It is well known that the luminescent properties of rare earth ions depend on the matrix in which these ions are placed: several studies have been performed on oxide hosts [2, 3, 5, 6, 7, 8], but all of them have revealed a too strong non-radiative decay from the $^3P_0$ level, quenching the starting laser level. Continuous wave laser action has been demonstrated in $YAlO_3$ [9], but the best results have been obtained in fluoride materials [10, 11, 12] in both pulsed and cw regime, because of the low phonon energy. The first laser experiments used Xe flashlamps or Ar^+-lasers as pumping sources; recently the development of the solid state technology has greatly enhanced the emission using laser diodes or optically pumped semiconductor lasers (OPS) as pumping sources [13, 14].

In Refs. [10, 11, 12, 13, 14], visible laser action has been demonstrated in $LiYF_4:Pr^{3+}$. In this work we will focus our attention on the isomorphous crystal $Pr:LiLuF_4$ (Pr:LLF). In that anisotropic fluoride host, Pr ions enter the Lu^{3+} S4 site in the scheelite-like tetragonal structure. The differences with respect to the well known YLF consist in the shorter distance of the S4 sites, leading to a closer position of the Pr ions, but on the opposite LLF possesses phonons with lower cut-off energy, larger emission cross sections and the possibility to grow congruently, resulting in a higher optical quality of the grown crystal. In particular we will report on the growth, emission and absorption spectroscopy and laser action at four different wavelengths. For every laser experiment Findlay-Clay and Caird analysis have been carried out in order to fully characterise the cavity and the crystal quality. To the best of our knowledge the reported slope efficiencies are the highest reached for a Pr-based laser so far.

1.1. Crystal-growth

The crystal growth apparatus consists of a home-made Czochralski furnace with conventional resistive heating; special care has been devoted to the quality of the vacuum system, which has an ultimate pressure limit better than 10^{-7} mbar, and the growth process was carried out in a high-purity (99.999%) argon atmosphere. The 5N powders, as well as their purification from OH^- contamination, have been provided by AC Materials (Tampa, Fl., USA).

The sample was grown using LiF and LuF_3 powders as raw material for the host and a proper amount of PrF_3 powder has been added for achieving the 1.25% nominal doping in the melt. The growing conditions were 5 RPM for the rotation rate and the pulling rate 1 mm/h, and the
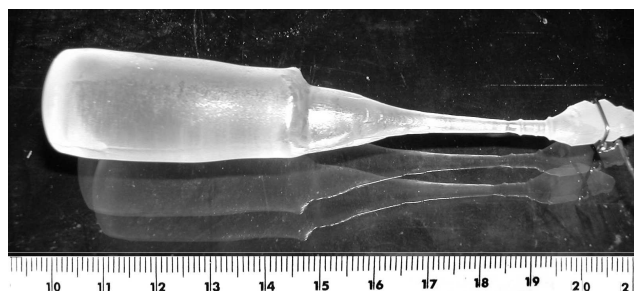

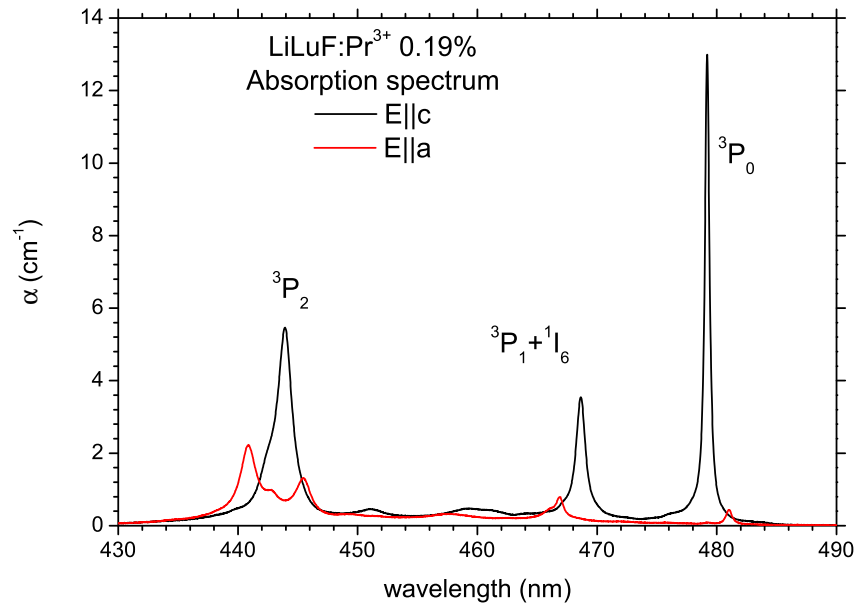Fig. 2. Picture of the boule of $LiLuF_4:Pr^{3+}$ sample as grown.

Fig. 3. Room temperature polarized absorption spectra of LiLuF$_4$:Pr. The maximum absorption is 13 cm^{-1} in the $E \parallel c$ polarization at 479.2 nm with a FWHM of 0.46 nm.

temperature of the melt was ≈860 °C. The furnace is also provided with an optical apparatus for automatic diameter control. The size of the crystal was about 12 mm in diameter and 55 mm in length (see Fig. 2). The single crystalline character of the sample was checked using a X-ray Laue technique that allows us to identify the c-crystallographic axis and cut oriented samples since the optical characteristics strongly depend on the position of the optical axes. Samples of two different lengths (4.07 mm and 9.20 mm) have been prepared. The crystal end faces (≈3×3 mm^2) were polished for laser quality.

ICP analysis has been performed on the sample in order to ascertain the actual doping concentration. In fact it is well known that, due to the ionic radius mismatch between Pr and Lu, the segregation coefficient is lower than one: in our case it has been measured a 0.19% as actual doping concentration against the 1.25% Pr content in the melt.

1.2. Spectroscopy: experimental set-up and results

The polarized absorption spectra were measured by a CARY 500 spectrophotometer between 240 and 2400 nm with a resolution of 0.1 nm in the UV-VIS wavelength region and 1 nm in the NIR region. In Fig. 3 the result obtained for the σ and π polarization are shown in the region where the $^3P_2$, $^3P_1+^1I_6$ and $^3P_0$ manifolds peaks lies; in particular the $^3P_0$ absorption as a maximum of 13 cm^{-1} in the $E \parallel c$ polarization at 479.2 nm with a FWHM of 0.46 nm.

Room temperature polarized emission measurements have been performed between 460 and 740 nm by exciting the samples using the 457.9 nm radiation from a cw Argon laser pumping the $^3P_1+^1I_6$ manifolds with a pump power as little as 3 mW. For the emission measurements, the laser beam was focused onto the samples with a 10 cm focal length lens. The fluorescence signal was detected perpendicularly to the pump laser direction to avoid pump spurious
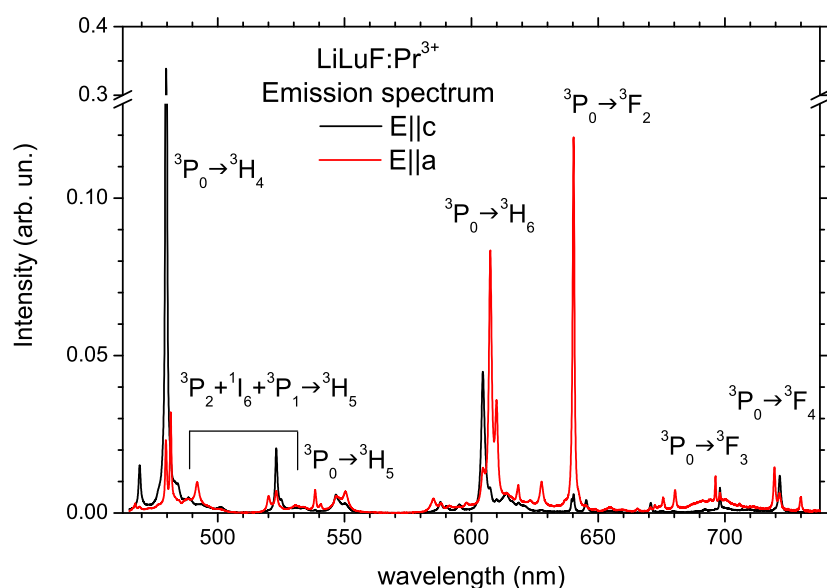
Fig. 4. Room temperature polarized emission spectra of Pr:LLF.

scattering. The luminescence was chopped and focused by a 75 mm focal length Infrasil lens on the input slit of a *Jobin-Yvon* monochromator with 320 mm focal length, equipped with a Glan-Thomson polarizer at the entrance in order to perform polarized measurements. For the fluorescence measurements we used a 1200 gr/mm grating blazed at 500 nm, and the resolution was set to 0.13 nm. The signal was filtered by proper filters (λ_t=460 nm) in order to suppress as much as possible any spurious laser scattering from the sample; the fluorescence was detected by a R1464 Hamamatsu photomultiplier, fed into pre-amplifiers, processed by a lock-in amplifier and subsequently stored on a PC. The acquired spectra were normalized for the optical response of the system using a black-body source at 3000 K.

The results are shown in Fig. 4: as can be seen the spectra are reach in features and several transition lines are present; for sake of clarity only some of them have been labelled. The emission of the Pr:LLF is dominated by the transitions starting from the $^3P_0$ level; in particular the most intense line lies in the blue region of the spectrum at 479.6 nm corresponding to the $^3P_0 \rightarrow ^3H_4$ transition to the ground state. Using the absorption data, the Füchtbauer-Ladenburg formula allows us to calculate the emission cross sections at the lasing wavelength; the results are reported in Tab. 1.

Table 1. Emission cross section of Pr:LLF at the lasing wavelengths.

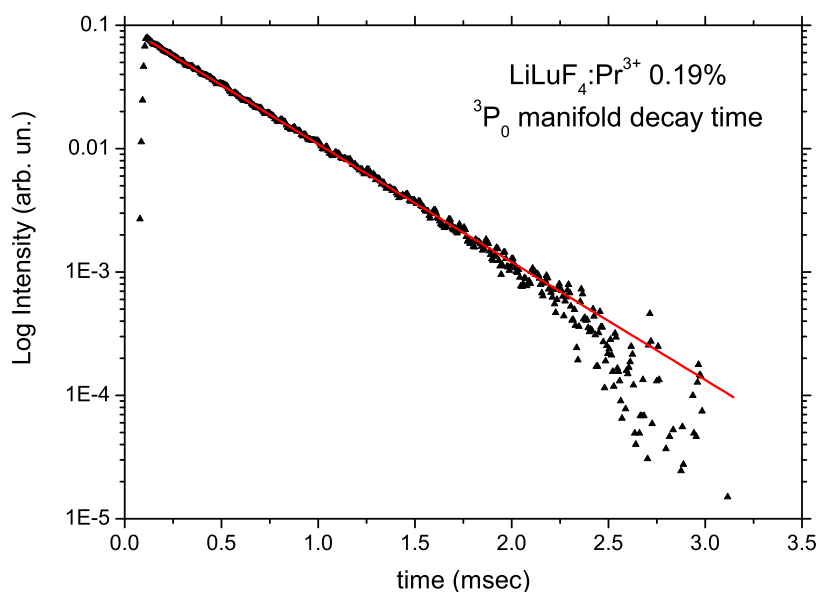| λ (nm)	σ_{em} (10^{-19} cm^2)
522.8	0.3
607.2	1.4
640.2	2.2
721.5	0.9

Fig. 5. Decay time curve of the $^3P_0$ manifold in Pr:LLF.

Room temperature decay time behaviour of the starting laser level, i.e. the $^3P_0$ manifold. It has been recorded with an apparatus similar to that described for the steady state measurements, but in this case the pumping source was a frequency doubled pulsed tunable $Ti:Al_2O_3$ (pulse duration $\approx$ 30 ns) laser tuned to the maximum absorption of the $^3P_2$ manifold around 442 nm. The sample was pumped near an edge and the fluorescence was collected from a thin section ($\approx$ 1 mm) of the sample to observe a uniformly pumped volume and reduce radiation trapping effect. Furthermore the power incident on the sample was reduced by means of attenuators to suppress non-linear effects as much as possible; we estimated the incident energy as little as 10 nJ. The signal from the photomultiplier was amplified, by fast amplifiers, and then processed by a digital oscilloscope, connected to a PC for storing purpose.

As can be seen in Fig. 5, the decay time curve exhibits a single exponential behaviour that has been fit with τ=45.4 $\pm$ 0.3 μs. This result is in agreement with that of Ref. [1], where the authors have measured 48 μs in a 0.026% Pr-doped LLF.

2. Laser setup and results

The pump process was done by a cw frequency-doubled OPS laser (Coherent Lübeck GmbH, Lübeck, Germany), providing a linear polarized beam at 480 nm wavelength with nearly diffraction limited emission ($M^2 \approx$ 1). The wavelength of the OPS was tuned to 479.5 nm for optimal absorption in the Pr:LLF laser crystal. The maximum output power available at this wavelength was 220 mW. This laser was only slightly tunable and it does not allow us to reach the absorption peak lying at 479.2 nm: for this reason 479.5 nm have been chosen as pumping wavelength (it was the shortest reachable wavelength) where the maximum output power was 220 mW. The pump laser was focused on the sample by a 50 mm focal length lens, resulting in a spot size of 28 μm and confocal parameter of 12 mm. Uncoated Pr:LLF sam-

ples have been placed in a concentric resonator (cavity length≈90 mm, mirrors radii: 50 mm, confocal parameter: 24 mm) with their c-axis parallel to the pump laser polarization. For all the experiments proper input couplers have been used, having high transmission at the pump wavelength and high reflectivity at the lasing wavelength; in order to perform a detailed analysis of the different laser transitions, several output couplers were used for every experiment. For all the experiments the pumping wavelength and the laser emission have been measured with a Fourier-transform-spectrometer: the spectral stability have been checked repeating several times the wavelength measurements also in different days, resulting always in the same value within the experimental error. Regarding the temporal laser stability, the output power has been monitored resulting in a rms noise of less than 2% over 2 hours.

2.1. 640.2 nm: $^3P_0 \rightarrow ^3F_2$ transition

The first laser transition that has been measured was the "red" one around 640 nm corresponding to the $^3P_0 \rightarrow ^3F_2$ transition. Only for that experiment two different sample thickness have been used in order to determine the optimal crystal length, 4.07 mm and 9.20 mm respectively. In both cases the output wavelength was 640.17 nm and was σ-polarized, in agreement with the intensity shown in Fig. 4. The results for the two samples under investigation are reported in Tab. 2. As it is evident, the best performances have been obtained for the shortest sample for both slope efficiency and threshold power, and the subsequent laser experiments have been performed only for that one. This result is consistent with the absorbtion measurements of the $^3P_0$ level shown in Fig. 3: at λ=479.47 nm (pumping wavelength), the absorption coefficient is α=5.4 cm^{-1}, resulting in 89% absorption for the 4.07 mm sample and in more than 99% for the longer one; furthermore a longer sample gives rise to higher scattering losses.

Table 2. Comparison of the laser results of the 4.07 mm and 9.2 mm long samples for the laser emission at 640.2 nm.

	4.07 mm		9.2 mm	
T_{oc} (%)	η_{abs} (%)	P_{thr} (mW)	η_{abs} (%)	P_{thr} (mW)
1	34	10	26	31
2	46	17	38	40
4	54	27	44	61
6	56	39	42	78

The analysis of the results for the 4.07 mm sample, reported in Fig. 6, shows that the lowest threshold is equal to 10 mW using a T=1% output coupler, the maximum output power 52.7 mW and the maximum slope efficiency η_{abs}=56%. To the best of our knowledge this is the highest slope efficiency reported up to now in the literature for Pr-based crystals. In Fig. 7 the Findlay-Clay and Caird analysis are reported: both methods indicate a value for the round trip losses equal to 0.4%. Furthermore the Caird analysis suggest a maximum theoretical slope efficiency of 65%; this result is not very far from the maximum value shown in Fig. 6 and Tab. 2.

The best performances of the longer samples were 31 mW as lowest threshold value (three-times more than the 4.07 mm sample) and a maximum slope efficiency of 44% and a maximum output power of 38.9 mW. Findlay-Clay and Caird analysis have been done also for the 9.20 mm long crystal: here we do not report the corresponding figures, but the values are in agreement with those of the shortest sample. This first result for the losses value certifies for the high optical quality of the crystal; for comparison in Ref. [11] the losses value measured for a Pr:YLF sample were 1.5%. The results are reported in Tab. 3 together with those at the other wavelengths; in addition, for every transition under investigation, we report the overlap efficiency (calculated as the ratio between the maximum possible slope obtained by the Caird
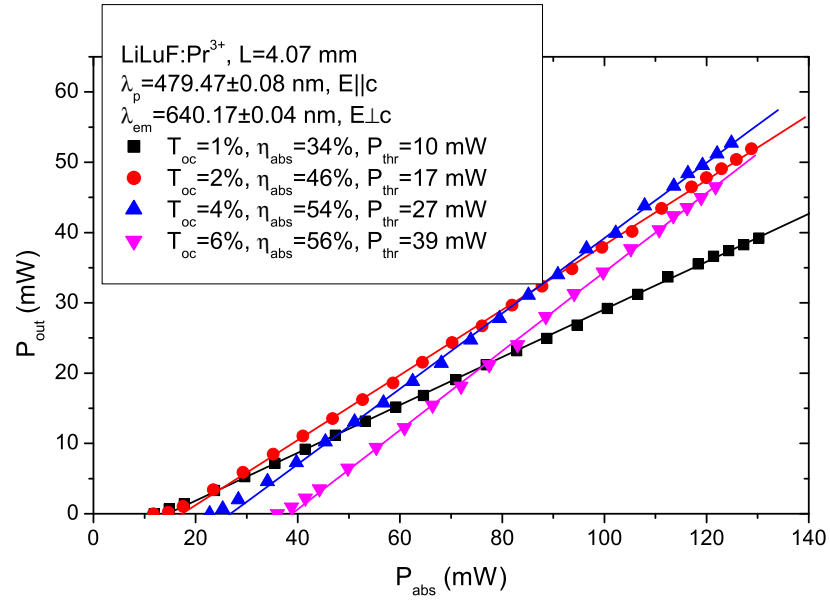
Fig. 6. Output power at 640 nm as a function of the absorbed power for the 4.07 mm long Pr:LLF sample.
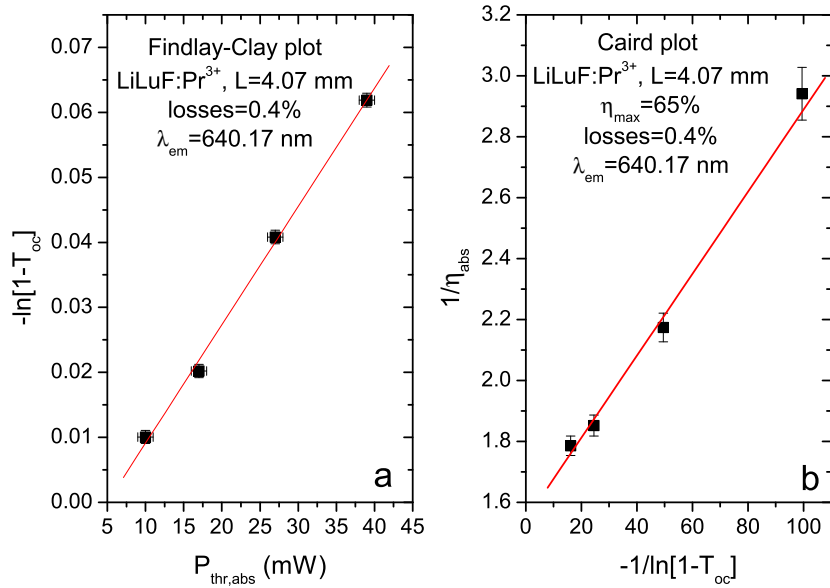

Fig. 7. Findlay-Clay (a) and Caird (b) analysis of the laser emission at 640 nm for the 4.07 mm long Pr:LLF crystal.

analysis and the quantum defect of the transition) and the optical conversion efficiency (i.e. the ratio between the maximum output power and the maximum incident power).

2.2. 721.5 nm: $^3P_0 \to ^3F_4$ transition

The second most intense transition in Pr is the one around 720 nm corresponding to the $^3P_0 \to ^3F_4$ transition. The output wavelength was 720.5 nm and also in this case was in σ-polarization. The output power characteristics are shown in Fig. 8. The minimum threshold was 12 mW using a T=0.72% output coupler and the maximum output power 50 mW with η_{abs}=46%.

Also in this case Findlay-Clay and Caird analysis have been performed and the results are reported in Tab. 3. The obtained value for the round trip losses were 0.3% for both methods, in agreement with the results obtained for the 640 nm laser. The Caird analysis indicates a maximum slope efficiency equal to 57%, and also in this case the agreement with the experimental value is satisfactory.
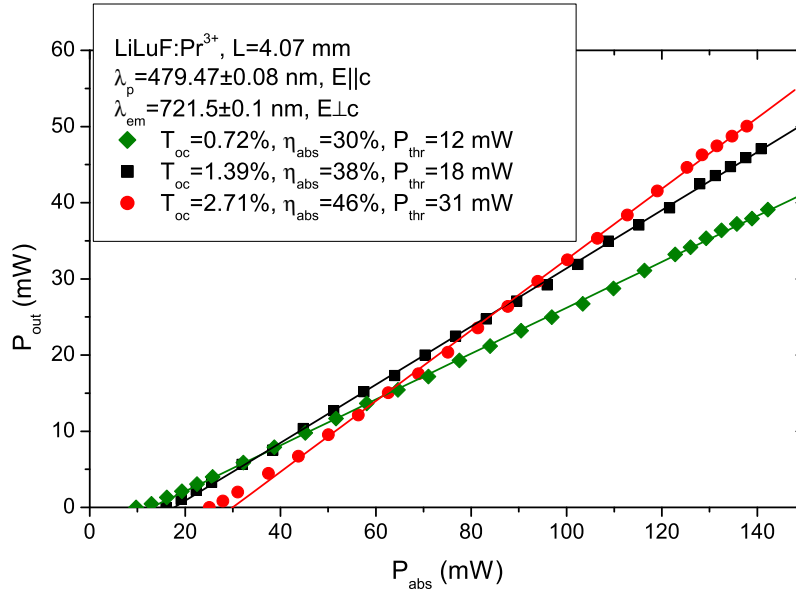

Fig. 8. Output power at 720 nm as a function of the absorbed power for the 4.07 mm long Pr:LLF sample.

2.3. 607.2 nm: $^3P_0 \to ^3H_6$ transition

The last transition under analysis originating from the $^3P_0$ level was in the orange region around 607 nm having as final laser level the $^3H_6$ manifold. Fig. 9a shows the output characteristics as a function of the absorbed power: in this case the emission line was at 607.25 nm but it was in π-polarization. In this case the maximum output power was 34.5 mW with a maximum slope efficiency of 31% and also the threshold was twice than the previous cases being 26 mW with T=1.13% as output coupler.

The different behaviour of this transition is also reflected by the results of the Findlay-Clay and Caird analysis: as can be seen from Tab. 3 the two method do not converge to an unique
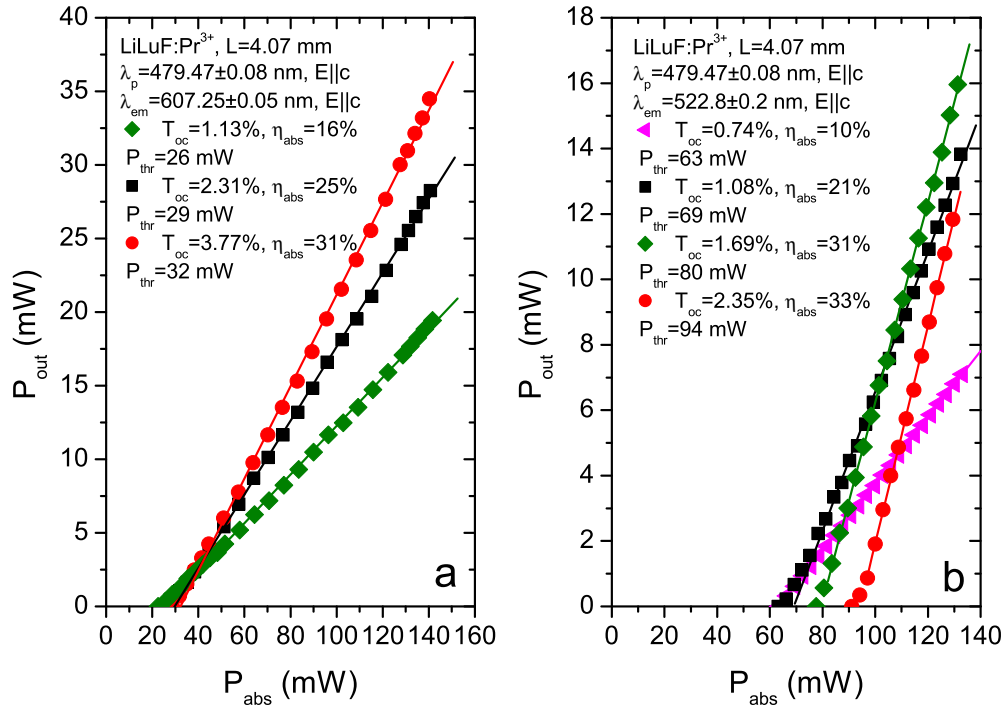
Fig. 9. Output power at 607 nm (a) and 522 nm (b) as a function of the absorbed power for the 4.07 mm long Pr:LLF sample.

value for the losses. Furthermore the value obtained with the Findlay-Clay analysis is one order of magnitude higher than the previous laser experiments for transition originating always from the $^3P_0$ level. The possible reason for this result are still under investigation: the possible candidates are a residual ground state absorption to the $^1D_2$ manifold or it can be ascribed to an excited state absorption at the laser wavelength starting from the $^3F_2$ or $^3F_3$ levels to the $^3P_2+^1I_6$ levels. Further measurements are in progress.

2.4. 522.8 nm: $^3P_1 \rightarrow ^3H_5$ transition

The last laser experiment was in the green region around 523 nm corresponding to the $^3P_1 \rightarrow ^3H_5$ transition. The $^3P_1$ manifold is thermally populated from the $^3P_0$ level being the energy difference only 550 cm^{-1}, that can be easily bridged at room temperature (200 cm^{-1}) by one phonon (for LLF $\omega_{phon}^{max} \approx 460$ cm^{-1} [12]). The different starting level of the laser transition reflects on the different output power characteristics shown in Fig. 9b; also in this case the π-polarized laser emission is in agreement with the spectroscopic data. Because of the indirect population mechanism of the upper laser level, the threshold power increases significatively to 63 mW also for an output coupler transmissivity of T=0.74%. With this output coupler the maximum power was 7.1 mW with η_{abs}=10%. This value increases with increasing transmission of the output coupler up to 33% with T=2.35%, the threshold became 94 mW and the output power reached 16 mW.

The different starting laser level has also consequences on the losses and slope efficiencies analysis. In fact Findlay-Clay plot (see Tab. 3) gives 1.3% as value for the round trip losses while the Caird analysis indicates 0.9%. The increased losses value (at least three times that of the 640 nm and 721 nm laser emission) can be ascribed to the shorter lifetime value of the $^3P_1$ manifold.

Table 3. Summary of the laser results of Pr:LLF as a function of the emission wavelength for the 4.07 mm long sample. In addition the overlap efficiency and the optical conversion efficiency are reported.

λ_{em} (nm)	P_{out}^{max} (mW)	η_{abs}^{max} (%)	T_{oc} (%)	P_{thr}^{min} (mW)	Findlay-Clay losses (%)	Caird losses (%)	η^{max} (%)	overlap effi-ciency (%)	optical conversion efficiency (%)
640.2	52.7	56	6	10	0.4	0.4	65	86.8	30
721.5	50.0	46	2.71	12	0.3	0.3	57	85.8	26
607.2	34.5	31	3.77	26	5.3	1.2	51	64.6	18
522.8	16.0	33	2.35	63	1.3	0.9	61	66.5	6

3. Conclusions and further developments

In conclusion, we reported on the growth of a Pr:LLF crystal and on the spectroscopic analysis we have performed regarding absorption and emission in both steady state and dynamical regime. We demonstrated efficient continuous-wave laser emission at room temperature in a Pr:LLF sample on several transitions in the green, orange, red and near-infrared spectral ranges, with the highest slope efficiencies for all the transitions, to the best of the authors knowledge. The Findlay-Clay and Caird analysis have been performed for every laser experiment: the low value for the round trip losses demonstrates the high optical quality of the grown crystal. The further development will consist in the power scaling of the system and in the possibility to obtain efficient intracavity UV frequency doubling exploiting the resistance to color center formation of the LLF crystal.